Article

Not peer-reviewed version

Laser-Driven Ion Sources Generated by Ns Laser Pulses at the Intensity Range of 10^{13}–10^{15} W/cm^2

Lorenzo Giuffrida *, Valeriia Istokskaia, Antonino Picciotto, Vasiliki Kantarelou, Mario Barozzi, Rosanna Dell`Anna, Martin Divoký, Ondrej Denk, Damiano Giubertoni, Filip Grepl, Asenios Hadjikyriacou, Martin Hanus, Josef Krása, Milan Kucharik, Tadzio Levato, Petr Navratil, Jan Pilar, Francesco Schillaci, Stanislav Stancek, Marco Tosca, Maksym Tryus, Andriy Velyhan, Antonio Lucianetti, Tomáš Mocek, Daniele Margarone

Posted Date: 24 July 2023

doi: 10.20944/preprints202307.1571.v1

Keywords: Laser-Plasma Ion Sources; High Power Laser Applications; Ion Diagnostics

Article

Laser-Driven Ion Sources Generated by ns Laser Pulses at the Intensity range of 10^{13}–10^{15} W/cm^2

L. Giuffrida [1,*], V. Istokskaia [1,2], A. Picciotto [3], V. Kantarelou [1], M. Barozzi [3], R. Dell`Anna [3], M. Divoky [4], O. Denk [4], D. Giubertoni [3], F. Grepl [1,2], A. Hadjikyriacou [1,2], M. Hanus [4], J. Krasa [5], M. Kucharik [2], T. Levato [1,†], P. Navratil [4], J. Pilar [4], F. Schillaci [1], S. Stancek [1,6], M. Tosca [1,7], M. Tryus [1], A. Velyhan [1], A. Lucianetti [4], T. Mocek [4] and D. Margarone [1,8]

[1] ELI Beamlines Facility, The Extreme Light Infrastructure ERIC, Dolní Břežany, Czech Republic
[2] Czech Technical University in Prague, Faculty of Nuclear Sciences and Physical Engineering, Prague, Czech Republic
[3] Micro-Nano Facility, Sensors and Devices, Fondazione Bruno Kessler, Trento, Italy
[4] HiLASE Centre, Institute of Physics of the Czech Academy of Sciences, Dolní Břežany, Czech Republic
[5] Institute of Physics ASCR, v.v.i (FZU), Prague, Czech Republic
[6] Joint Laboratory of Optics of Palacky University, Institute of Physics of Academy of Sciences of the Czech Republic, Faculty of Science, Palacky University, Olomouc, Czech Republic
[7] Charles University in Prague, Faculty of Mathematics and Physics, Department of Macromolecular Physics, Prague, Czech Republic
[8] Centre for Plasma Physics, School of Mathematics and Physics, Queen's University Belfast, Belfast, United Kingdom
* Correspondence: Lorenzo.Giuffrida@eli-beams.eu
† Currently at Advanced Material Research Center, Technology Innovation Institute, Masdar City, Abu Dhabi, UAE.

Abstract: An experimental platform for laser-driven ion (sub-MeV) acceleration and potential applications was recently commissioned at the HiLASE laser facility. The auxiliary beam of the Bivoj laser system operating at GW peak power (~10 J in 5-10 ns) and 1-10 Hz repetition rate enabled a stable production of high-current ion beams of multiple species (Al, Ti, Fe, Si, Cu, Sn). The produced laser-plasma ion sources were fully characterized against the laser intensity on target (1013-1015 W/cm2) by varying the laser energy, focal spot size, and pulse duration. This allowed to provide accurate scaling laws of the maximum ion energy for the different target materials investigated. Such experimental scaling laws are presented for the first time in the investigated laser intensity range and for ns-class laser pulses, and allow to provide a qualitative interpretation of the laser-plasma interaction underpinning physics, thus to tune the main features of the accelerated ion beams (energy, temperature, and current). Such a detailed study was facilitated by the large amount of data acquired at high repetition rate (1-10 Hz) provided by the Bivoj laser system. The versatility and tuneability of such high-repetition-rate laser-plasma ion sources are of potential interest for multidisciplinary user applications.

Keywords: Laser-Plasma Ion Sources; High Power Laser Applications; Ion Diagnostics

1. Introduction

Soon after the first demonstration in 1960`s of the laser from a ruby crystal [1], various laser systems started to be massively used in different research fields. In 1970's, the possibility to focus a pulsed laser beam into a solid medium to generate sources was recognized as a very promising field of research [2,3]. In 1990's, laser technologies were able to demonstrate the generation of very short pulses (few tens of femtoseconds). In addition, thanks to the recent discovery of the Chirped Pulse Amplification (CPA) technique [4], it became possible to concentrate relatively high laser energy in ultra-short pulses, thus enabling the rapid development of TW and PW laser systems [5].

 doi:10.20944/preprints202307.1571.v1

Currently, laser driven ion sources are being considered as a complementary and compact approach for the generation of ion sources with unique features (e.g. peak current, short bunch duration, high charge state, and low emittance) compared to conventional accelerators. Consequently, a strong effort of the laser-plasma scientific community has been put in the optimization of such non-conventional ion sources (energy, flux, stability) based on key requirements for their potential use in societal applications, such as cancer treatment ([6,7]), energy production from inertial confinement fusion [8] and cultural heritage [9].

Recently, the availability of table-top, fs-class laser systems operating at relatively low peak power (TW level) but at high repetition rate (10 Hz to 1 kHz) has opened new exiting directions of research, including acceleration of ions with moderate energies (MeV-level), but high average flux and high stability [10,11]. On the other hand, table-top, ns-class laser systems operating at a repetition rate of ~10 Hz and delivering 0.01-1 J laser energy on target have been widely used in the last decades to produce high current ion sources with low energies at laser intensities in the range of 10^{10}-10^{12} W/cm^2, ([12–14]). Applications in the field of Pulsed Laser Deposition [15], Laser Induced Breakdown Spectroscopy [16], nanoparticle production [17], laser implantation [18], and generation of laser ion sources [19] call for special requirements in terms of ion source performances to be optimized prior to the given experiment.

This work is based on the commissioning phase of an experimental area available for users at the HiLASE laser facility (Czech Republic), which offers the capability to use the auxiliary beam of the Bivoj laser system (10 J, 5-10 ns in FWHM, and 1-10 Hz) focused on solid targets at laser intensities up to 10^{15} W/cm2 to generate and subsequently use the ion sources of different species and energies. To the best of our knowledge, available data on laser-plasma ion sources refer to the intensity range of 10^{13}-10^{15} W/cm2 which is achieved solely using kJ-class nanosecond (or sub-ns) laser pulses [20,21], which typically operate in single shot regime. Furthermore, in vision of future multidisciplinary applications, a parametric study of such laser-driven ion sources is required to evaluate the versatility and tuneability of such particle beams through appropriate experimental scaling laws. We note that the possibility to generate stable ion beams at high repetition rate (up to 10 Hz) enables to acquire a large amount of experimental data, thus to minimize statistical uncertainties coming from laser-plasma shot-to-shot fluctuations in order to build robust and reliable scaling laws. In addition, hydrodynamic simulations (HD) were performed with the main objective to support the interpretation of the experimental results.

2. Experimental setup

The experimental platform is located in the user open access area at the HiLASE laser facility. It consists of an in-air optical setup for a shot-to-shot characterization of the laser beam, a vacuum chamber and a set of online diagnostics for the ion source characterization. A sketch of the experimental apparatus is depicted in Figure 1a.

Preprints (www.preprints.org) | NOT PEER-REVIEWED | Posted: 24 July 2023 doi:10.20944/preprints202307.1571.v1

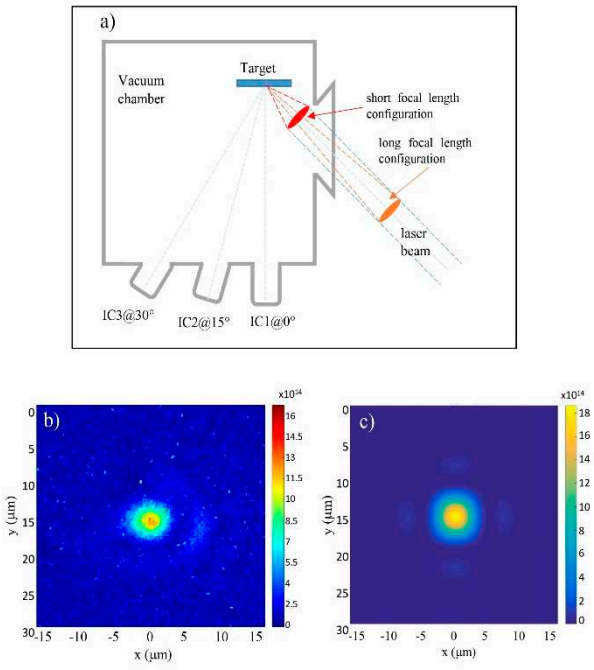

Figure 1. a) Schematic of the experimental setup for the two possible optical geometries: the short focal lens (in red) and the long focal lens (in orange) setups. Three Ion Collectors (IC1, IC2 and IC3) are placed at different angles to monitor the angular distribution of the accelerated ions. b) and c) show the experimental and theoretical (simulated) laser beam spatial distributions in the focal plane (target position). The color scale in each laser spot represent the laser intensity (in W/cm^2).

The auxiliary beam of the Bivoj laser system (22x22 mm^2) available for users at this experimental platform allows to deliver up to 10 J at the fundamental wavelength of 1032 nm and with pulse width tunable from 5 to 10 ns (super-Gaussian). Additionally, the temporal pulse profile can be shaped with 100 ps resolution based on the specific user requirements [22]. In the following discussion, if not explicitly specified, the laser beam is assumed having a super-Gaussian spatial profile of the 14th order.

Two different optical setups were used to focus the laser beam on target:

- 100-mm short focal lens geometry (lens placed inside the vacuum chamber);
- 500-mm long focal lens geometry (lens placed outside the vacuum chamber).

The short focal lens (f = 100 mm) configuration allowed to reach a maximum intensity on target above 1.4x10^{15} W/cm^2. An example of the laser focal spot measured by a microscopic objective system is presented in Figure 1b. Figure 1c shows a numerical estimation of the laser spot in the focal plane performed by the Virtual Lab Fusion software that returned a value of 4.2 m, whilst the experimental spot was 5.5 m. This corresponds to a laser peak intensity of 2x10^{15} W/cm^2 at an energy of 4.5 J on target, which is very close to the experimental.

However, the use of the short focal lens implies limitations in the total number of laser shots on target due to the large amount of debris generated during the laser-target interaction that are deposited on the lens surface after each shot, thus deteriorating the lens performance after a certain number of shots.

In contrast, the long focal lens optical setup resolves this issue and makes possible to fire an unlimited number of shots on target, although the maximum achievable laser intensity was reduced to about 4x10^{14} W/cm^2.

The used cubic vacuum chamber (50x50x50 cm^3) is modular in terms of flanges and viewports available for the connections of various plasma diagnostics directly aiming at the interaction point. Furthermore, thanks to the intentionally small chamber volume, the overall pumping time (from atmospheric pressure to ~10^{-5} mbar) is much less than 30 min.

 doi:10.20944/preprints202307.1571.v1

The target is mounted onto a rotating holder that allows to operate up to a repetition rate of 10 Hz, thus allowing to fire several thousands of laser shots in a single experimental run [23]. The device has two motors, a linear stage for lateral movements, and a rotation stage (the combination of both movements makes an imprint on the target surface that is similar to a spiral). The monitoring system used for the alignment of both the laser beam and the target on the focal plane is an Infinity Corrected Long Working Distance Objective with 10X magnification, connected to a tube lens 200 mm and a CCD camera.

Three Ion Collectors (ICs) were placed at 0°, 15°, and 30° with respect to the target normal to provide a shot-to-shot full characterization of the ion source by the time-of-flight (TOF) technique [24]. The laser-target angle of incidence was 45°.

The experimental results reported in this work were performed using thick targets (several mm in thickness), thus accelerating ions only in the backward direction, i.e. from the target front surface.

The online ion diagnostics were benchmarked with results estimated using ex-situ techniques. In fact, a good agreement between the results from the TOF diagnostics and the estimation carried out using the SIMS (Secondary Ion Mass Spectrometry analysis) technique carried out on a sample implanted with ions from the laser plasma source was demonstrated. For this specific measurement, the Bivoj laser beam was focused with an intensity of 1.4×10^{15} W/cm^2 onto a Fe target. The laser accelerated Fe ions were implanted on Si substrates (2x2 cm^2) placed at 10 cm distance from the Fe target and at different angles with respect to the target normal, and simultaneously monitored online by the IC-TOF diagnostics.

An example of a TOF spectrum recorded by the IC placed at 15° (63 cm away from the target) and obtained during a run of 3600 laser shots is shown in Figure 2a. The TOF spectrum shows an intense and narrow photo-peak used as start signal (0 ns), which corresponds to X-ray plasma radiation produced by the laser-target interaction. It is followed by a broad signal, corresponding to XUV radiation coming from electron recombination processes in the plasma. The beginning of the peak ascribable to ions at about 0.4 s corresponds to protons (the fastest positively charged particles in the plasma) and shows maximum energies of ~10 keV. The most intense and broad part of the signal ascribable to Fe ions and other contaminants present on the target surface (mainly hydrocarbons) starts at ~1 s, which returns a maximum Fe ion energy of 65 keV. Since ion signals of different species in the TOF spectra can overlap with each other's, a technique of signal decomposition was applied to distinguish the different components [24]. Figure 2a shows the original TOF spectrum (black line) and the signal (dashed red line) obtained using the revelation of the individual ion components (proton signal in green, C ion signal in orange, and Fe ion signal in blue). Such analysis also allowed to estimate a total Fe ion flux of ~ 1×10^{11} ions/cm^2 at 10 cm from the target.

Preprints (www.preprints.org) | NOT PEER-REVIEWED | Posted: 24 July 2023 doi:10.20944/preprints202307.1571.v1

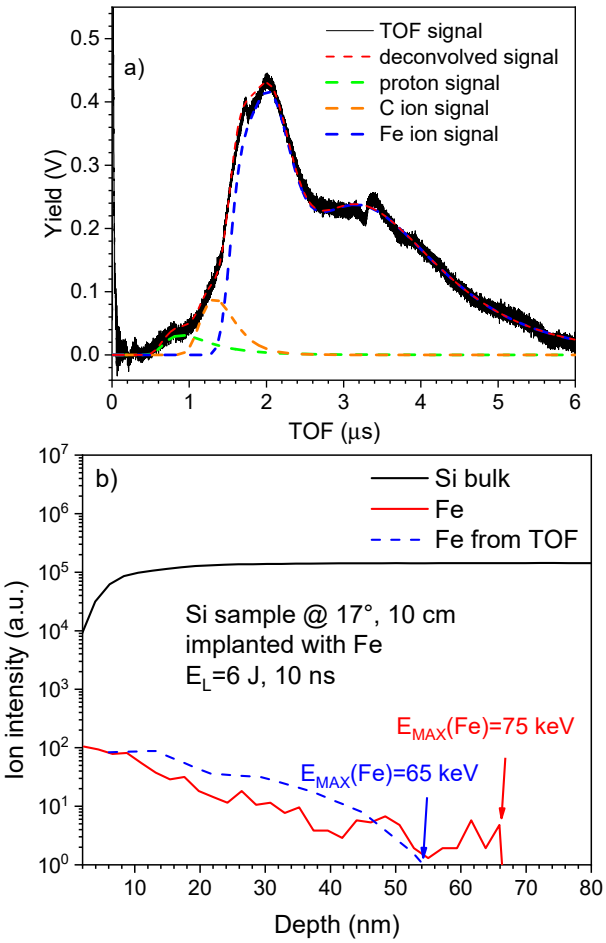

Figure 2. a) TOF spectrum ions recorded with an IC at 63 cm from the target and angle of 15° with respect to the target normal. The Fe target was irradiated with a laser intensity of 1.4*10[15] W/cm[2]. The decomposition of the signal into subcomponents (red dashed line) is in good agreement with the TOF signal (black line). For completeness, the proton (green), C (orange), and Fe ion signals (blue) are also shown. b) SIMS analysis of a Si sample placed at 17° with respect to the target normal implanted with Fe ions with a maximum energy of 75 keV. For comparison, the blue dashed line is shown to represent the depth profile obtained by the IC detector reported in a).

After ion implantation, all the samples were accurately characterized at Fondazione Bruno Kessler (FBK). Figure 2b shows a result from the SIMS analysis performed in one of the irradiated Si sample placed at 10 cm from the target and at 17° with respect the target normal and implanted with laser accelerated Fe ions. The ion intensity profile (relative intensity vs depth of the implantation) for the Si substrate (black line) and the implanted material (Fe in red line) are shown.

The estimated penetration range of Fe ions into the Si substrate between 60 and 70 nm corresponds to a maximum Fe ion energy of 75 keV (calculated using the Monte Carlo based software SRIM [25].

Additionally, the SIMS analyses allowed to estimate the flux that was 3.4x1010 Fe ions/cm²/shot. Both values (maximum ion energy and ion flux) are in good agreement with those found from the TOF analyses. The penetration depth of Fe ions shown in blue in Figure 2b is estimated from the energy distribution extracted from the TOF signal using the SRIM code to convert the Fe ion energy into the corresponding range in the Si substrate. As shown, the calculated Fe ion range matches very well the one measured via SIMS analyses.

3. Results

The first test was performed using the short focal lens configuration with the goal to reach the smallest possible laser spot at the interaction point (around 5.5 m in FWHM), as shown in Figure

Preprints (www.preprints.org) | NOT PEER-REVIEWED | Posted: 24 July 2023 doi:10.20944/preprints202307.1571.v1

1b. The laser energy was varied from 0.5 J to 6 J for a given pulse duration of 10 ns, thus allowing to modulate the laser intensity on target in the range $2.4x10^{14}$ – $1.4x10^{15}$ W/cm^2. In this experimental run, a 2-mm thick Al target was used.

Some examples of TOF spectra recorded at different laser energies/intensities by the ICs placed at 0° a), 15° b), and 30° c) are shown in Figure 3. It is worth to note that the amplitudes of such spectra are normalized at 1 m detection distance for an immediate comparison among detectors placed at different distances. In general, the ion signal is faster (early beginning of the TOF spectrum) when higher laser energies are used and when the detector is closer to the target normal (small detection angle).

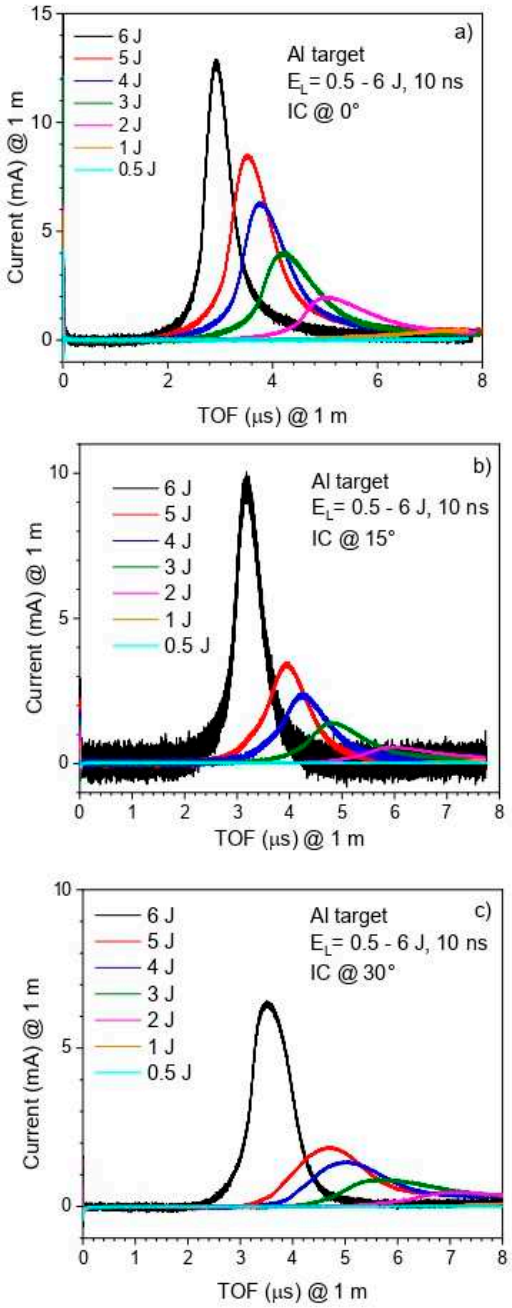

Figure 3. Example of TOF spectra from IC detectors placed at 0° a), 15° b) and 30° c) recorded after the interaction of the Al target with the Bivoj laser beam at different energies and 10 ns pulse duration. Each spectrum has been normalized at an ideal distance of 1 m for comparison.

Preprints (www.preprints.org) | NOT PEER-REVIEWED | Posted: 24 July 2023 doi:10.20944/preprints202307.1571.v1

Moreover, at a given laser energy, the ion signal amplitude decreases when reducing the detection angle (e.g., in the case of 6 J laser energy, the ion current corresponding to the main peak decreases from ~13 mA at 0° to ~6 mA at 30°).

The long focal lens (f = 500 mm) configuration was used in all the remaining experimental runs to avoid technical issues related to target debris contamination. This setup is appropriate for long irradiation intervals at high repetition rate, e.g. in case of user applications in the field of laser-driven ion implantation [26,27].

The main drawback of the long focal lens setup is the relatively large focal spot compared to the short focal lens case (around 13 μm FWHM in diameter), which causes a drop in laser intensity down to ~7x10^{14} W/cm^2 (for a laser energy of 6 J). Laser parameter scans (energy and pulse duration) were carried out with the goal to investigate the scaling laws for the ion cutoff energy and ion flux.

A summary of all the experimental runs performed with an Al target is shown in Figure 4a,b. The ion cutoff energy and flux normalized to 10 cm detection distance was studied for 5 ns (in red), 10 ns (in black), and 9 ns (but Gaussian temporal profile, in blue) pulse widths. The experimental values shown in Figure 4 are averaged over 10 consecutive shots obtained in the same laser/target conditions and measured by the IC placed at 0°.

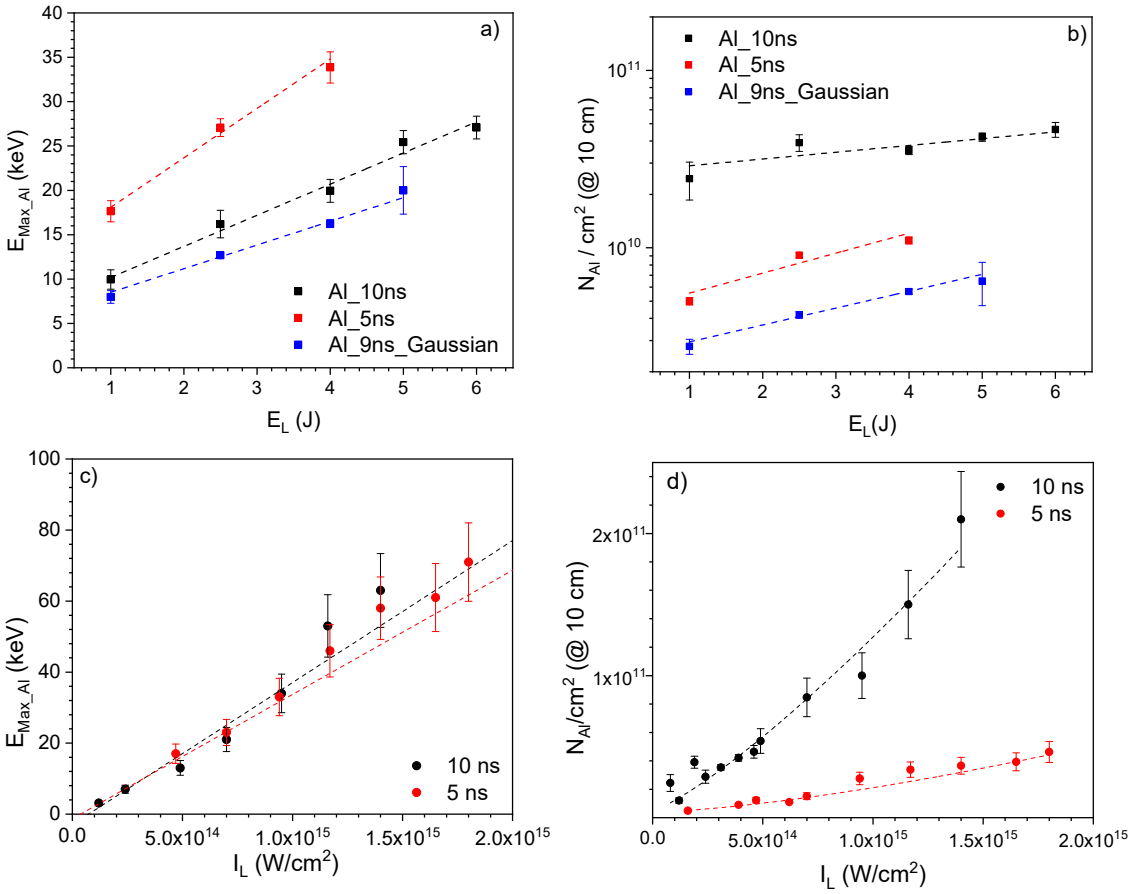

Figure 4. Al ion cutoff energy a) and ion flux normalized to 10 cm detection distance b) for different laser energies and pulse durations (5 ns and 10 ns super-Gaussian shape, and 9 ns Gaussian temporal shape). Fig c) and d) show the dependence of the Al ion cutoff energy and ion flux on the laser intensity, respectively.

Figure 4a reports the maximum Al ion energies for the different laser energies in the case of 5 ns and 10 ns super-Gaussian and for the case of 9 ns Gaussian temporal profile. For a given laser energy, the shorter the pulse width the higher the maximum ion energy, which can be easily linked to the corresponding higher laser intensity. Similarly, for a given pulse duration, the maximum ion energy increases proportionally to the laser energy.

The fit of experimental points has been done using the following linear formula:

Preprints (www.preprints.org) | NOT PEER-REVIEWED | Posted: 24 July 2023 doi:10.20944/preprints202307.1571.v1

$$E_{\max\_Al} = a + b * E_L \quad (1)$$

where E_{max_Al} is the maximum Al ion energy, E_L is the laser energy and a and b are fitting parameters. The slope of the curve b is ranging from 2.7±0.2 (9 ns Gaussian case) to 5.6±0.6 (5 ns case) and an intermediate value of 3.5±0.2 for the 10 ns case.

On the other hand, the longer the pulse duration the higher the ion flux (Figure 4b). A longer pulse duration (target irradiation time) can be associated to a plasma sustained for a longer time, thus to a larger amount of material emitted from the surface, including the flux of the accelerated ions.

Figure 4c shows the relation between the maximum Al ion energy and the laser intensity. The plot clearly shows that the ion energy does not depend on the laser pulse width. Both data sets can be fitted using the same fitting curve:

$$E_{Max\_Al} = a_1 * (I_L)^{b_1} \quad (2)$$

showing an almost linear behavior in both cases (b_1 is equal to 1.11±0.06 and 1.21±0.07 respectively for the case 5 ns and 10 ns).

Moreover, the ion flux strongly depends on the pulse duration as it is shown in Figure 4d, where it appears to be much larger in the case of 10-ns pulse width.

Figure 4a,b clearly show that the use of a Gaussian pulse is much less efficient than a super-Gaussian one, both in terms of ion cutoff energy and ion flux. The use of hydrodynamic simulations HD with the 2D cylindrical Arbitrary Lagrangian-Eulerian code PALE [28] supports such experimental findings.

Figure 5 shows a comparison of HD simulations obtained using a Gaussian (9 ns pulse width at FWHM) and a super-Gaussian (10 ns at FWHM) laser pulse. Figure 5a–c show the Al density profile evolution at three different times (2ns, 6 ns, and 10 ns, respectively) after the interaction of the laser beam with the target. The laser beam comes from the top of each plot and propagates along the z-direction into the Al target (target normal direction). The target front surface is thus positioned at z = 0 m.

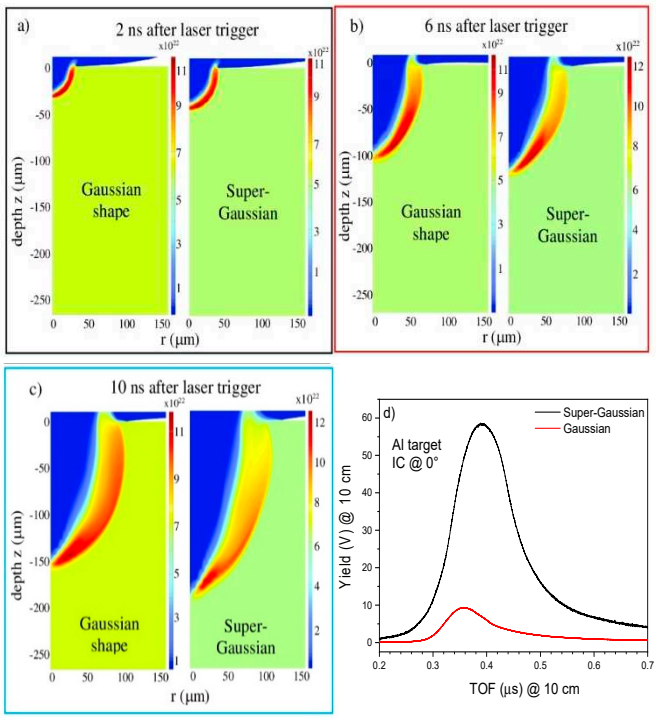

Figure 5. HD simulations comparing Gaussian vs super-Gaussian temporal laser pulse shapes at three different time after the laser interaction, respectively 2 ns a), 6 ns b), and 10 ns c). TOF spectra from Al ions generated by the interaction of an Al target with a Gaussian and a super-Gaussian temporal shape d).

Preprints (www.preprints.org) | NOT PEER-REVIEWED | Posted: 24 July 2023 doi:10.20944/preprints202307.1571.v1

The simulation outputs show that 2 ns after the laser-target interaction (Figure 5a) the crater on the Al surface is slightly deeper in the super-Gaussian pulse case. Such difference largely increases after 6 ns (Figure 5b), and even more at 10 ns (Figure 5c). The super-Gaussian temporal profile is very steep, thus delivering almost all the energy exactly in 10 ns. Vice versa, the Gaussian shape distributes the energy in a broader time. Ultimately, the super-Gaussian pulse supports a more efficient interaction with the target than the Gaussian one. This feature can be clearly seen in the ion density profile calculated numerically: a much larger ablated volume appears in the super-Gaussian case. This is also confirmed experimentally as reported in Figure 4a,b.

For completeness, Figure 5d reports the comparison of TOF spectra obtained in both cases by using the same IC detector with the laser parameters used in the HD simulations. The TOF spectrum recorded from ions generated by a super-Gaussian pulse (in black) shows a much higher signal than the Gaussian case (in red). Moreover, that TOF signal starts to raise much earlier for the super-Gaussian pulse, thus demonstrating a clear enhancement of the maximum ion energy, as previously summarized in Figure 4.

4. Discussion

A full characterization of the ion source is mandatory for its optimization and for a deep understanding of the underlying physical processes that regulate the laser-plasma interaction and subsequent ion acceleration. One of the key plasma parameters that can be indirectly extracted from the TOF spectra is the ion temperature kT_i. To accomplish this goal, a dedicated experimental run consisting of series of consecutive laser shots onto Cu targets in the intensity range $1x10^{13}$ - $6x10^{13}$ W/cm^2 was conducted. The recorded TOF spectra were post-processed to estimate the ion temperature, using the following fit function [29,30]:

$$i(t) = A * \frac{d^2}{t^5} exp\left[-\frac{m_i}{2kT}\left(\frac{d}{t} - v_S\right)^2\right] \quad (3)$$

where i(t) is the ion current, A a normalization coefficient, d is the flight distance, m_i the ion mass, t the detected TOF, v_S the velocity shift, and kT_i the ion temperature.

The obtained results are summarized in Figure 6a, reporting the relationship between the ion temperature kT_i and the laser irradiance IL^2 using a fit function of the type:

$$kT_i \propto (I_L\lambda^2)^{\delta} \quad (4)$$

where is the fitting parameter. The best fit returned a parameter 0.311±0.005 as shown in Figure 6a. The inset shows a good agreement of such a fit function with a data point acquired at the highest laser intensity of $1.4x10^{15}$ W/cm^2 (short focal lens setup). To the best of our knowledge, there are no similar studies reported in the literature in such laser energy and intensity regimes where the predominant laser-absorption mechanism is inverse bremsstrahlung [31].

Preprints (www.preprints.org) | NOT PEER-REVIEWED | Posted: 24 July 2023 doi:10.20944/preprints202307.1571.v1

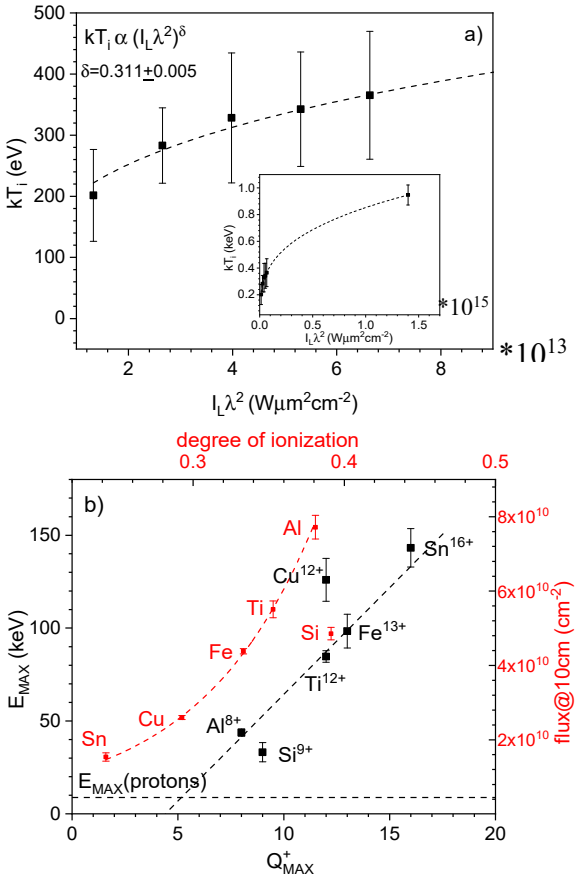

Figure 6. a) Cu ion temperature kT_i vs. laser irradiance $I_L\lambda^2$. A fitting function of the type $kT_i \alpha (I_L\lambda^2)^{\delta}$ matches very well the experimental data when $\delta=0.311\pm0.005$. b) Ion flux vs. degree of ionization (in red), and maximum ion energy vs maximum ion charge state (in black) for different target materials at the laser intensity of 7×10^{13} W/cm^2.

An additional goal of our work was to perform a systematic study of the performances of the laser-plasma ion sources generated with different target materials at a laser intensity of about 1×10^{13} W/cm^2. This was achieved thanks to a statistically robust investigation showing that light element targets (e.g. Al) can produce substantially higher ion fluxes compared to heavy element ones (e.g. Sn). This can be qualitatively explained by the observation that low-Z materials have higher degrees of ionization compared to high-Z materials, thus leading to the generation of larger ion fluxes. Such a dependence is shown in Figure 6b. The red dashed line refers to the measured ion flux against the degree of ionization of the different target materials. On the other hand, the black dashed line shows a linear dependence of the experimental ion cutoff energy versus the calculated maximum ion charge state.

At the laser intensity of interest (of the order of 10^{13} W/cm^2), Inverse Bremsstrahlung is the main laser absorption mechanism occurring in the plasma. A qualitative picture of the overall acceleration process in the investigated experimental conditions is presented in the followings.

During the first stages of the laser-target irradiation, electrons are isotropically heated and start to collide with other charged particles in the produced plasma. The plasma heated by such collisional absorption on the target front side, expands into the half-space away from the target plane. Since protons are the lightest positively charged species in the plasma, they leave the target earlier than other ion species, thus they are accelerated with an average kinetic energy that does not strongly depend on the target composition, but mainly on the laser intensity (this is also shown in Figure 6b reporting a constant trend for the maximum proton energy for different target materials). Ultimately, at the end of the laser interaction, the plasma heating process ends and a local space-charge effect is generated within the plasma Debye length. As a results, the highly charged ions are further pushed

 doi:10.20944/preprints202307.1571.v1

away from the high density, positively charged plasma region, i.e. they acquire additional kinetic energy due to Coulomb repulsion effects that depend on the effective ion charge state. As a result of this mechanism, the final ion energy would not (or only slightly) depend on the plasma (electron) temperature but on the Coulomb repulsion which is more effective for high ion charge states. This is confirmed by the experimental results summarized in Figure 6b. The maximum ion energies are recorded for the ions with the highest charge states, whilst the proton energy is basically independent of the target material.

5. Conclusions

Results from the commissioning experiment of the laser-plasma ion source platform at the HiLASE Centre were presented. The 10-J auxiliary beam of the ns-class Bivoj laser system was operated at high repetition rate (up to 10 Hz), thus demonstrating the capability of such experimental platform to accommodate future user experiments requiring laser driven ion beams with energies up to 150 keV as a repetitive source for applications. Various target materials (Al, Ti, Fe, Si, Cu, and Sn) were investigated in the laser intensity range of 10^{13}-10^{15} W/cm^2 (5-10 ns pulse width) with the goal of demonstrating the versatility of the produced laser-plasma ion sources, but also to present for the first time to the best of our knowledge the corresponding experimental scaling laws for the maximum ion energy, thus to provide a qualitative interpretation of the underpinning physics.

The described results represent a statistically robust experimental study enabled by the high repetition rate capability of the experimental chain (laser system, target refreshing device, ion diagnostics, data acquisition, and real-time data analysis), which allowed to average the laser-plasma shot-to-shot fluctuations out, thus to investigate the experimental scaling laws and consequently tune the ion source parameters.

The ion source features demonstrated experimentally at high repetition rate are of high interest for future user applications. For example, ion implantation in various user samples requires an overall ion dose in the substrate of the order of 10^{15} atoms/cm^2. In fact, a proof-of-principle demonstration of such application was realized assuming the implantation of 10^{15} Al ions/cm^2 into a Si substrate at a depth of 500 Å as user requirement, the laser-driven ion source was operated for ~30 minutes at a repetition rate of 10 Hz. The result of such a continuous ion implantation is shown in Figure 2. The Al ions with energies up to 30 keV (generated using the Bivoj laser beam with 6 J on target and 10-ns pulse width) were directed into a Si substrate placed 10 cm away from the target. (~5x10^{10} ions/cm^2/shot).

Another potential user application is pulse laser deposition (PLD) on large samples, e.g. coating various materials with homogenous or nanostructured layers of the desired material (e.g. carbon) [32].

Furthermore, the commissioned laser-plasma ion sources show unique characteristics in terms of ion beam current in the order of few Amperes in the energy range of several tens of keV, as shown in Figure 7. This is of high relevance in the field of laser ion sources (LIS). In fact, heavy ions with high charge state can be injected into a radiofrequency cavity [33,34] for post acceleration. In particular, the ion source characterized in the present manuscript can produce much-higher current with respect to the previously cited work (where the injected current is in the order of few hundred of mA per shot) which is of interest for application requiring accelerators that can deliver relatively high beam power.

Preprints (www.preprints.org) | NOT PEER-REVIEWED | Posted: 24 July 2023 doi:10.20944/preprints202307.1571.v1

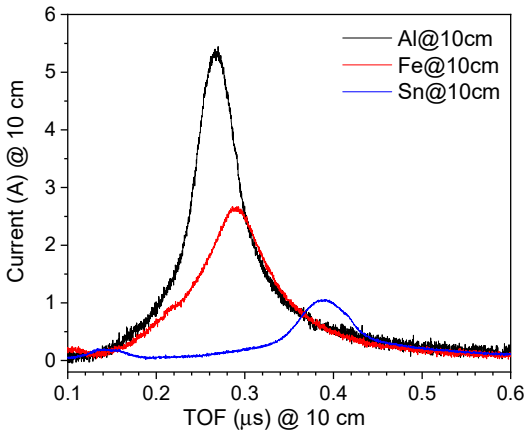

Figure 7. Example of TOF spectra after the interaction between an Al (black), Fe (red), and Sn (blue) targets with the Bivoj laser. The corresponding energies are specified in Figure 6b (several tens of keV).

As a potential perspective, the 100 J arm of the Bivoj laser system, could be used to enhance the performances of the laser-driven ion source. In fact, considering the same laser characteristics in terms of pulse duration and spot size as in the 10 J arm, the 10x higher laser energy would allow to reach a 10x higher laser intensity of the order of 10^{16} W/cm^2. As a result, higher ion energies could be reached (~400 keV considering the scaling law from formula (2) extracted from Figure 4c) and, thus, pave the way towards additional applications (i.e. [35]).

Author Contributions: Conceptualization: LG, AP, AL, TM and DM; Setup preparation: LG, FG, MTr, FS, AV; Software: IV, SS, AH, MK, TL; Laser operation: MD, OD, MH, JP and PN; Experiment running: LG, MTo, FS, SS, VI and AV; Data analysis: LG, VI, AP, VK, MB, DA, DG, AH and SS; data evaluation: LG, DM and JK; writing—original draft preparation: LG and DM; writing—review and editing: all authors; supervision: LG and DM; project preparation: LG, AP, DM, AL and TM; funding acquisition: DM, MK, TM. All authors have read and agreed to the published version of the manuscript.

Funding: This work has been supported by the Ministry of Education, Youth, and Sports of the Czech Republic by the Project No. LQ1606 and by the project Advanced Research Using High Intensity Laser Produced Photons and Particles (CZ.02.1.01/0.0/0.0/16_019/0000789). M. Kucharik was supported by the Czech Science Foundation project 19-24619S, the European Regional Development Fund project CZ.02.1.01/0.0/0.0/16_019/0000778, the EUROfusion project CfP-FSD-AWP21-ENR-01-CEA-02, and RVO 68407700. This work was co-financed by the European Regional Development Fund and the state budget of the Czech Republic (project HiLASE CoE: Grant No. CZ.02.1.01/0.0/0.0/15_006/0000674) and by the Royal Society International Exchange funding scheme (project No. IES/R2/203175).

Conflicts of Interest: The authors declare no conflict of interest.

References

1. Maiman T. H. Stimulated Optical Radiation in Ruby. Nature 187 493–4 (1960).
2. Peacock N. J. and Pease R. S., Sources of highly stripped ions. Journal Physics D: Appl. Phys. 2: 1705 (1969).
3. Nuckolls J. et al., Laser Compression of Matter to Super-High Densities: Thermonuclear (CTR) Applications. Nature 239 139–142 (1972).
4. Strickland D. and Mourou G., Compression of amplified chirped optical pulses, Opt. Commun. 56 (1985).
5. Danson C. N. et al., Petawatt and exawatt class lasers worldwide. High Power Laser Science and Engineering , Volume 7 , e54 (2019).
6. Bulanov S.V. and Khoroshkov V.S., Feasibility of using laser ion accelerators in proton therapy, Plasma Physics Reports, 28, 5 (2002).
7. Yogo A. et al. Measurement of relative biological effectiveness of protons in human cancer cells using a laser-driven quasi mono energetic proton beamline, Appl. Phys. Lett. 98, 053701 (2011).
8. Zylstra A.B., et al., Burning plasma achieved in inertial fusion. Nature 601, 542–548 (2022).

9. Barberio M. et al., Laser-Accelerated Proton Beams as Diagnostics for Cultural Heritage, Sci Rep. 7, 40415 (2017).
10. Morrison J. T. et al., MeV proton acceleration at kHz repetition rate from ultra-intense laser liquid interaction, New J. Phys. 20 022001 (2018).
11. Levy D. et al., Low-divergence MeV-class proton beams from kHz-driven laser-solid interactions, https://arxiv.org/pdf/2112.12581.pdf
12. Torrisi L. et al., Comparison of Pd plasmas produced at 532 nm and 1064 nm by a Nd:YAG laser ablation, Nuclear Instruments and Methods in Physics Research B 268, 13 (2010).
13. Kashiwagi H. et al., Nd–YAG laser ion source for direct injection scheme, Review Of Scientific Instruments 75, 5 (2004).
14. Rosinski M. et al., Laser produced streams of Ge ions accelerated and optimized in the electric fields for implantation into SiO2 substrates, Review of scientific instruments 83, 02B305 (2012).
15. Wang L. et al., Manipulating redox reaction during pulsed laser deposition. J. Appl. Phys. 118, 185305 (2015).
16. Stavropoulos P. et al., Laser-induced breakdown spectroscopy as an analytical tool for equivalence ratio measurement in methane-air premixed flames. Spectrochimica Acta, Part B 59, 1885 (2004).
17. Mangione A. et al., Carbon nanocrystals produced by pulsed laser ablation of carbon, Radiation Effects & Defects in Solids, Vol. 160, Nos 10–12, 655–662 (2005).
18. Giuffrida L. et al., Ge Post-Acceleration from laser-generated plasma. Nuclear Instrument and Methods A. 623 (2010).
19. Kanesue T. et al., Laser ion source with solenoid field. Appl. Phys. Lett. 105, 193506 (2014).
20. Jungwirth K., Recent highlights of the PALS research program. Laser and Particle Beams 23, 2 (2005).
21. L. Laska et al., Charge-state and energy enhancement of laser-produced ions due to nonlinear processes in preformed plasma. Applied Physics Letters 86, 081502 (2005).
22. Pilar J., et al. Characterization of Bivoj/DiPOLE 100: HiLASE 100-J/10-Hz diode pumped solid state laser. Proc. SPIE 10511, Solid State Lasers XXVII: Technology and Devices, 105110X (2018); https://doi.org/10.1117/12.2290290.
23. Chagovets T. et al., Automation of Target Delivery and Diagnostic Systems for High Repetition Rate Laser-Plasma Acceleration. Appl. Sci. 11, 1680, (2021).
24. Margarone D. et al., Full characterization of laser-accelerated ion beams using Faraday cup, silicon carbide, and single-crystal diamond detectors. Journal of Applied Physics 109, 103302 (2011).
25. www.srim.org
26. Rosinski M. et al., Laser generated Ge ions accelerated by additional electrostatic field for implantation technology. Applied Surface Science Vol 272 109– 113, (2013).
27. J. Krasa et al., Energy spectra of Ag, Au, Sn, and Pb ions emitted from laser-created plasmas determined from their implantation depth profile in a metallic substrate. Laser and Particle Beams 20, 109–112 (2002).
28. Liska, R. et al., ALE Method for Simulations of Laser-Produced Plasmas. In: Fořt, J., Fürst, J., Halama, J., Herbin, R., Hubert, F. (eds) Finite Volumes for Complex Applications VI Problems & Perspectives. Springer Proceedings in Mathematics, vol. 4 (2011). Springer, Berlin, Heidelberg. https://doi.org/10.1007/978-3-642-20671-9_87
29. Krasa J. et al., Repetitive outbursts of fast carbon and fluorine ions from sub-nanosecond laser-produced plasma. Laser and Particle Beams 27, 171–178 (2009).
30. Picciotto A., et al., Plasma temperature and ion current analysis of gold ablation at different laser power rates. Nuclear Instruments and Methods B, 247 (2006) 261-267.
31. Eliezer S., The interaction of high-power lasers with plasmas. CRC press, (2002).
32. Maffini A. et al., Production of Carbon Nanofoam by Pulsed Laser Deposition on Flexible Substrates. Carbon Materials: Chemistry and Physics 11 pp 135-157, https://doi.org/10.1007/978-3-030-81827-2_7
33. Sako T. et al., Development of C6+ laser ion source and RFQ linac for carbon ion radiotherapy. Review of Scientific Instruments 87, 02C109 (2016).
34. Okamura M. Direct plasma injection scheme in accelerators, Review of Scientific Instruments 79, 02B314 (2008).
35. L. Romano et al., Nanostructuring in Ge by self-ion implantation. Journal of Applied Physics 107, 084314 (2010)